Title

A Material Basis Frame Approach for Global Deflection Reconstruction of Rod-Like Structures from Strain Measurements

ISBN

9783319152479

Author

Todd, Michael

Publication Date

2015

DOI

10.1007/978-3-319-15248-6_21

Peer reviewed

A Material Basis Frame Approach for Global Deflection Reconstruction of Rod-Like Structures from Strain Measurements

Michael Todd

Department of Structural Engineering, University of California San Diego, La Jolla CA 92093-0085;
email: mdtodd@ucsd.edu

ABSTRACT

This paper presents an approach for determining three-dimensional global displacement (for arbitrarily-sized deformations) of thin rod- or tether-like structures from a limited set of scalar strain measurements. The approach is rooted in exploiting a reference frame that is materially adapted, i.e., it moves with the cross section. Local linearization of the frame evolution equations is shown to yield local solutions that may be assimilated into a global solution via continuity relationships. The solution is shown to be robust to potential singularities from vanishing bending and twisting angle derivatives and from vanishing measured strain, and the approach includes strain resulting from pure neutral axis extension (such as due to thermal loads). Validation of the approach is performed through comparison with finite element simulations. The average root mean square reconstruction error of 0.01%-1% of the total length, for reasonable sensor counts. Analysis of error due to extraneous noise sources and boundary condition uncertainty shows how error scales with those effects.

Keywords: shape reconstruction, material basis frame, distributed strain, directors, Cosserat rod

1. INTRODUCTION

Many applications require monitoring the deflection of long, slender, highly flexible structures such as cables, long rods, tethers, or any structure whose geometry is dominated by a single length scale. Such structures all tend to share a kinematic state characterized by arbitrarily large multi-mode deflection (bending, twisting, torsion, extension) under relatively linear, elastic stress/strain material behavior. Euler is credited with initiating studies in the *Elastica*, followed by more modern theories [1-5]. In most structural monitoring applications of interest, a common objective is to obtain the displacement of the these structures from distributed measurements of some kind, whether the measurements are direct non-contact measures of displacement (such as with laser vibrometry), acceleration (requiring integration), or indirectly through distributed local measurements of a kinematically-related quantity, such as strain. This last approach comprises the scope of the present paper, since strain gages are a highly ubiquitous and a useful sensor modality for structural load and response. The main challenge in this class of monitoring problems lies in obtaining a reasonable inverse model that converts a finite number of local strain measurements into global displacement estimations. For small displacements of certain geometrically simple structural models for which analytical solutions exist (beams, plates), classical theories may be directly inverted or forward models may be fit to data directly, but no such viable method currently exists for long, highly-deformable structures. This paper presents a kinematic model rooted in Cosserat theory and introduces a material basis reference frame to describe the deformation more precisely in a way that measurable strain metrics are estimable from the theory. Then, under local linearization assumptions, the resulting displacement/material frame evolution equations are integrated in terms of the strain metrics to obtain global displacement. The approach is validated against several full finite element displacement simulations of a rod-like structure loaded to arbitrarily large deflections in this paper.

2. KINEMATIC MODELING AND SOLUTION APPROACH

Todd et al. [6] presented an earlier version of this approach that was limited to bending and twisting. The present approach has relaxed the previous assumptions and including extension of the centerline. Figure 1 (left) shows the geometry of an arbitrarily deformed structure with relevant length scales; the circular cross section shown is arbitrary, although the negligible warping assumptions made shortly will strictly only hold true for circular cross sections.

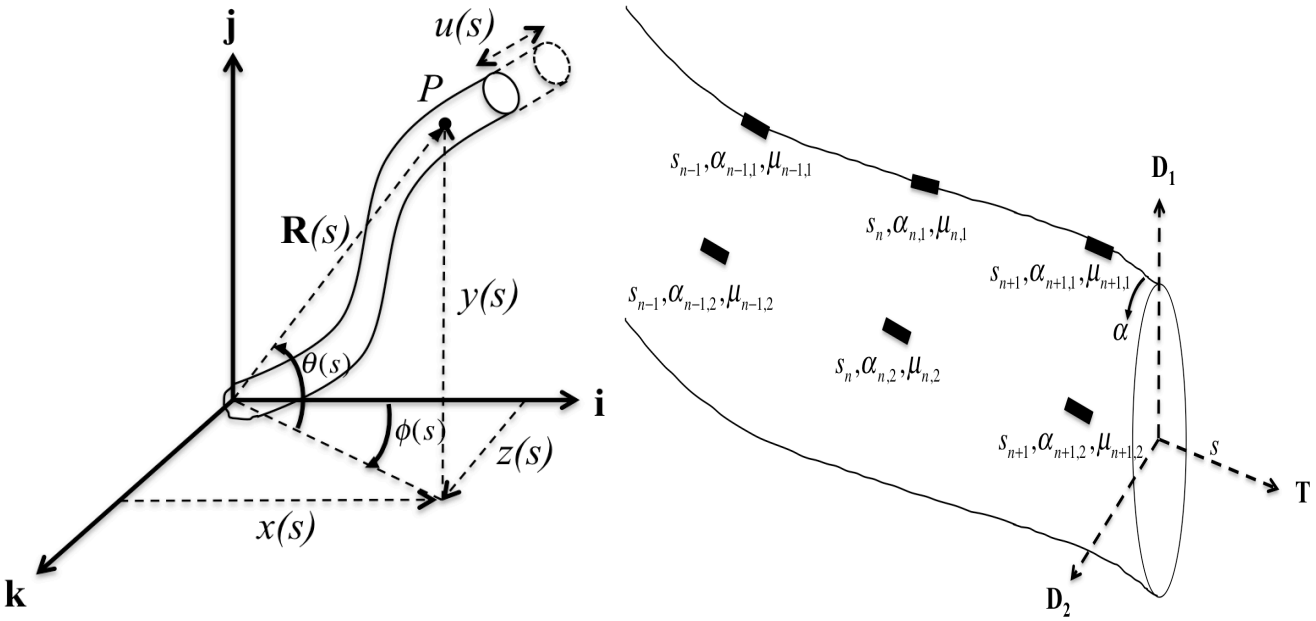

Fig. 1 (left) Fundamental geometric description of the deformed structure and (right) the geometry of the cross section.

The fundamental independent variable is the arc-length coordinate *s*, which moves along the tangent lin to the dominant length direction. An arbitrary point *P* on the centroid of the deformed structure may be described in the inertial **i-j-k** reference frame by parameterization of three functions, a pitch function $\theta(s)$, an azimuth function $\phi(s)$, and a stretch function *u(s).* The vector locator **R**(*s*) for *P* may be thus expressed as

$$\mathbf{R}(s)=\left(\int_0^s \cos\theta(p)\cos\phi(p)\left(1+u'(p)\right)dp\right)\mathbf{i}+\left(\int_0^s \sin\theta(p)\left(1+u'(p)\right)dp\right)\mathbf{j}+\left(\int_0^s \cos\theta(p)\sin\phi(p)\left(1+u'(p)\right)dp\right)\mathbf{k}, \quad (1)$$

where a prime mark denotes differentiation with respect to *s*. When there is no centerline stretching, i.e. $u'=0$, all deformation is due to bending and twisting, and the distal end of the structure resides on a sphere for all deformation possibilities (hence the spherical angular parameterization). When there is no bending or twisting, i.e. $\theta=\phi=0$, the vector **R** reduces to $\mathbf{R}(s)=\left(s+u(s)\right)\mathbf{i}$, which is just the location along the initially straight (undeformed) structure, plus any additional pure stretch. In the present formulation, it is assumed that the initial configuration is straight (for convenience) and unstrained (a more strict assumption). Furthermore, warping of the cross section of the structure and transverse shearing are neglected in the present approach.

While the vector **R**, written in the inertial basis, is sufficient to locate the loci of centroids, it does not successfully describe the material deformation about *P*, other than the case of pure stretch (as just shown in the previous paragraph). Thus, recourse is made to connecting **R** to a reference frame that is better adapted to the structure, i.e., it evolves with the deformation. The Frenet basis, consisting of a tangent vector **T**, a normal vector **N**, and a binormal vector **B**, is such an adapted frame, and its evolution is described by the well-known Frenet-Serrat equations, where all explicit dependences upon s are dropped for brevity:

$$\begin{bmatrix} \mathbf{R}' \\ \mathbf{N}' \\ \mathbf{B}' \\ \mathbf{T}' \end{bmatrix} = \begin{bmatrix} 0 & 0 & 0 & 1+u' \\ 0 & 0 & \tau & -\kappa \\ 0 & -\tau & 0 & 0 \\ 0 & \kappa & 0 & 0 \end{bmatrix} \begin{bmatrix} \mathbf{R} \\ \mathbf{N} \\ \mathbf{B} \\ \mathbf{T} \end{bmatrix}, \tag{2}$$

where κ and τ are the local curvature and torsion of the deformed centroid, both of which may be related back to complicated expressions involving the pitch, azimuth, and stretch functions by substituting Equation (1) into Equation (2). The Frenet basis, while useful, is nonetheless not material-adapted; rather, it is adapted to the curvature and torsion of the centroid and not to the actual physical bending and rotation of the material, which is what directly encodes the strain. As a consequence, the Frenet frame suffers discontinuities at inflection points, where **N** will vanish. This singularity in **N** prohibits its use in estimating local strain, which is not discontinuous. Thus, a material twist function $\sigma(s)$ is used to relate the **N**-**B** orientation at a particular cross section to a new vector basis $\mathbf{D}_1$-$\mathbf{D}_2$ that evolves with the cross section, as shown in Figure 1 (right). The definitions of $\mathbf{D}_1$ and $\mathbf{D}_2$ define the cosines of the two angle functions, $\mathbf{D}_1 \bullet \mathbf{j} = \cos\theta$ and $\mathbf{D}_2 \bullet \mathbf{k} = \cos\phi$, such that the material twist and its derivative are defined by

$$\begin{aligned} \kappa\cos\sigma &= -\phi'\cos\theta \\ \kappa\sin\sigma &= \theta' \\ \sigma' &= -\tau - \phi'\sin\theta \end{aligned}, \tag{3}$$

and Equation (2) may be rewritten in this new material-adapted reference frame as

$$\begin{bmatrix} \mathbf{R}' \\ \mathbf{D}_1' \\ \mathbf{D}_2' \\ \mathbf{T}' \end{bmatrix} = \begin{bmatrix} 0 & 0 & 0 & 1+u' \\ 0 & 0 & -\phi'\sin\theta & -\theta' \\ 0 & \phi'\sin\theta & 0 & -\phi'\cos\theta \\ 0 & \theta' & \phi'\cos\theta & 0 \end{bmatrix} \begin{bmatrix} \mathbf{R} \\ \mathbf{D}_1 \\ \mathbf{D}_2 \\ \mathbf{T} \end{bmatrix}. \tag{4}$$

Equation (4) clearly shows how the material-adapted frame encodes the pitch, azimuth, and stretch functions in its evolution description. In fact, these matrix components are the material-adapted frame's strain measures, which are obtained by

direct shear and axial:	bending and torsional:
$\mathbf{R}' \bullet \mathbf{D}_1 = 0$	$\frac{1}{2}\left(\mathbf{D}_1 \times \mathbf{D}_1' + \mathbf{D}_2 \times \mathbf{D}_2' + \mathbf{T} \times \mathbf{T}'\right) \bullet \mathbf{D}_1 = -\phi'\cos\theta$
$\mathbf{R}' \bullet \mathbf{D}_2 = 0$	$\frac{1}{2}\left(\mathbf{D}_1 \times \mathbf{D}_1' + \mathbf{D}_2 \times \mathbf{D}_2' + \mathbf{T} \times \mathbf{T}'\right) \bullet \mathbf{D}_2 = \theta'$
$\mathbf{R}' \bullet \mathbf{T} = 1+u'$	$\frac{1}{2}\left(\mathbf{D}_1 \times \mathbf{D}_1' + \mathbf{D}_2 \times \mathbf{D}_2' + \mathbf{T} \times \mathbf{T}'\right) \bullet \mathbf{T} = -\phi'\sin\theta$

(5)

The direct shearing strain measures are both zero, in accordance with the kinematic assumptions made earlier.

The total strain at the surface of the structure (where a strain gage could be arbitrarily located), say point Q in Figure 1 (right), is comprised of the orientation change in the coordinate system (which gives rise to bending and torsional strain) and any length change in the **T** direction (which gives rise to the axial strain). Thus, vector of non-zero strains in the material-adapted frame is given by

$$
\begin{aligned}
\boldsymbol{\varepsilon} &= \mathbf{r}'_{Q/P} + u'\mathbf{T} \\
&= r\cos\alpha\mathbf{D}'_1 + r\sin\alpha\mathbf{D}'_2 + u'\mathbf{T} \\
&= r\phi'\sin\theta\left(\mathbf{D}_1\sin\alpha - \mathbf{D}_2\cos\alpha\right) \\
&\quad + \left(u' - r\theta'\cos\alpha - r\phi'\sin\alpha\cos\theta\right)\mathbf{T}
\end{aligned}
\quad , \tag{6}
$$

where $\mathbf{r}_{Q/P}$ is the vector locating Q relative to P. This strain vector is then dotted with the orientation vector of an arbitrary strain gage, given by $-\sin\mu\sin\alpha\mathbf{D}_1 + \sin\mu\cos\alpha\mathbf{D}_2 + \cos\mu\mathbf{T}$ where μ is an angle relative to the $\mathbf{T}$ direction (i.e., a gage aligned in the tangential direction corresponds to $\mu = 0$). The final scalar strain at the point Q is then obtained by dotting Equation (6) with this gage orientation vector to obtain

$$
\begin{aligned}
\varepsilon &= \boldsymbol{\varepsilon} \bullet \left(-\sin\mu\sin\alpha\mathbf{D}_1 + \sin\mu\cos\alpha\mathbf{D}_2 + \cos\mu\mathbf{T}\right) \\
&= \cos\mu\left(u' - r\theta'\cos\alpha - r\phi'\cos\theta\sin\alpha\right) - r\sin\mu\phi'\sin\theta\,, \\
&= \cos\mu\left(e_1 - \cos\alpha e_2 - \sin\alpha e_3\right) - \sin\mu e_4
\end{aligned}
\tag{7}
$$

where the definitions of the strain metrics $e_m,\ m = 1...4$,

$$
\begin{aligned}
e_1 &= u' \\
e_2 &= r\theta' \\
e_3 &= r\phi'\cos\theta \\
e_4 &= r\phi'\sin\theta
\end{aligned}
\tag{8}
$$

were made.

It is then assumed that arrays of strain gages are placed on the surface of the structure, with each array having a gage at a discrete location $s = s_n$, circumferential position $\alpha = \alpha_{n,m}$, and orientation $\mu = \mu_{n,m}$, as shown in Fig. 2.,

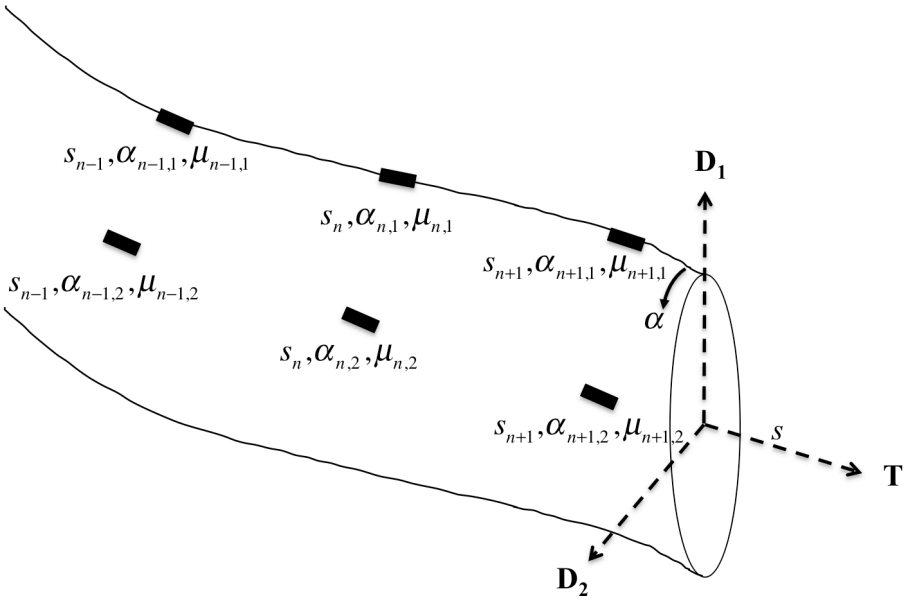

Fig. 2. Strain gage location nomenclature.

Thus, in the n-th cross-sectional neighborhood of each gage, Equation (4) may be written

$$\begin{bmatrix} \mathbf{R}_n' \\ \mathbf{D}_{1,n}' \\ \mathbf{D}_{2,n}' \\ \mathbf{T}_n' \end{bmatrix} = \begin{bmatrix} 0 & 0 & 0 & 1+e_{n,1} \\ 0 & 0 & -e_{n,4}/r & -e_{n,2}/r \\ 0 & e_{n,4}/r & 0 & -e_{n,3}/r \\ 0 & e_{n,2}/r & e_{n,3}/r & 0 \end{bmatrix} \begin{bmatrix} \mathbf{R}_n \\ \mathbf{D}_{1,n} \\ \mathbf{D}_{2,n} \\ \mathbf{T}_n \end{bmatrix}. \tag{9}$$

The predicted strain in Equation (7) for the *n*-th neighborhood may subsequently be written as

$$\varepsilon_{n,m} = \cos\mu_{n,m}\left(e_{n,1} - e_{n,2}\cos\alpha_{n,m} - e_{n,3}\sin\alpha_{n,m}\right) - \sin\mu_{n,m}e_{n,4}\,. \tag{10}$$

As it stands, Equation (9) is still nonlinear through the definitions made in Equation (8), but given a sufficient sensor density, it is assumed that the strain metrics $e_{n,j}$ are constant in their *n*-th neighborhood. Then, Equation (9) comprises a linear system with constant coefficients that may be solved. Defining $\gamma_n = \sqrt{e_{n,2}^2 + e_{n,3}^2 + e_{n,4}^2}$, the solution for the local position vector is

$$\begin{aligned} \mathbf{R}_n(s) = \mathbf{a}_{n,1} &+ \frac{\left(1+e_{n,1}\right)e_{n,4}\left(-\mathbf{a}_{n,3}e_{n,2} + \mathbf{a}_{n,2}e_{n,3} + \mathbf{a}_{n,4}e_{n,4}\right)}{\gamma_n^2}s + \frac{r}{\gamma_n^2}\left(1+e_{n,1}\right)\left(\mathbf{a}_{n,2}e_{n,2} + \mathbf{a}_{n,3}e_{n,3}\right)\left(1-\cos\left(\frac{\gamma_n s}{r}\right)\right) \\ &+ \frac{r}{\gamma_n^3}\left(1+e_{n,1}\right)\left(\mathbf{a}_{n,4}\left(e_{n,2}^2 + e_{n,3}^2\right) + e_{n,4}\left(\mathbf{a}_{n,3}e_{n,2} - \mathbf{a}_{n,2}e_{n,3}\right)\right)\sin\left(\frac{\gamma_n s}{r}\right) \end{aligned}, \tag{11}$$

where the $\mathbf{a}_{n,m}$ are vector constants of integration, and the strain metrics $e_{n,m}$ are linearly related to the actual measured strains $\varepsilon_{n,m}$ through Equation (10). Equation (11) represents the basis set solution, assuming locally constant strains, for the global displacement of the structure as a function of the measured strains. Similar-looking solutions with the same functional form but different integration constants describe the other vector components of Equation (9). The solution contains no obvious singularities other than potentially in the case of vanishing bending/torsional strain measures, i.e., $e_{n,m} = 0$ for *m*=2…4 (implying that $\gamma_n = 0$ also). However, a careful limiting process of Equation (11) shows that

$$\lim_{e_{n,2},e_{n,3},e_{n,4},\gamma_n \to 0} \mathbf{R}_n(s) = \mathbf{a}_{n,1} + \mathbf{a}_{n,4}\left(1+e_{n,1}\right)s\,, \tag{12}$$

which is a local linear stretch in the *s* direction only. Clearly, if there is also no stretching, i.e. $e_{n,1} = 0$, then $\mathbf{R}_n$ remains linear in the *n*-th neighborhood, but with a different slope. The situation of vanishing bending/torsional strain would only occur in situations where the derivatives of both θ_n and ϕ_n vanish simultaneously, implying a vanishing local curvature.

Thus, the algorithm proceeds by determining if all the measured strains at a given cross section are zero (or nearly zero by some tolerance) and then selects either the solution Equation (11) or (12) appropriately. Then, conditions of continuity between neighborhoods are imposed, along with boundary conditions, to fully determine the integration constants and arrive at a unique solution for the global displacement. The final displacement vector is then just assimilated by summing up over each *n*-th local contribution to get

$$\mathbf{R}(s) = \sum_{n=1}^{N} \mathbf{R}_n(s)\left[u\left(s - s_{n-1}^*\right) - u\left(s - s_n^*\right)\right], \tag{13}$$

where the s_n^* are the locations chosen to impose continuity between regions (a typical choice may be the midpoint between strain sensors), and $u(*)$ is the Heaviside function.

Although not absolutely required if global displacement is all that is needed, the local pitch, azimuth, and stretch functions may be computed from Equation (8) to be

$$u_n = a_n + e_{n,1} s$$
$$\theta_n = b_n + e_{n,2} s / r \quad , \tag{14}$$
$$\phi_n = c_n + \frac{e_{n,3}}{e_{n,2}} \sin\theta_n - \frac{e_{n,4}}{e_{n,2}} \cos\theta_n$$

where the a_n, b_n, and c_n are integration constants whose values are also determined by imposing continuity and boundary-related conditions on these functions (consistent with whatever other conditions were imposed).

3. VALIDATION OF THE APPROACH

The proposed described was tested on finite-element based simulation of large deformations of a hollow plastic pipe of length 50 m, inner diameter 20 cm, and outer diameter 30 cm. The material constants chosen were an elastic modulus E=2.3 GPa and Poisson's ratio ν=0.39. Abaqus S4R general-purpose shell elements were employed to model this structure, given their superior capability and computational efficiency in modeling large-scale bending and torsional behavior. Four strain gages at each cross section were simulated at 90^{O} separation circumferentially (α direction) and alternating orientations (μ) of $\pm 45^{\mathrm{O}}$. There is nothing optimal about this arrangement, but the use of 4 fibers with orientation diversity adds robustness; if μ=0 is chosen to orient all gages, then in principle only 3 strain gages at each cross section would be required. In all cases, the gage clusters were spread at 50/N m apart, i.e., uniformly spaced.

Figure 3 shows the results of the reconstruction approach for one simulation that contained only two major changes in curvature/torsion (and negligible stretch). The finite element simulation of the cylinder centerline is shown as the solid black line (the dashed black line is the initially straight, undeformed cylinder), and the gray line is the continuous reconstruction from the algorithm of Section 2. For this first shape, even for just N=5, fairly good reconstruction is observed, with an average (over the total length) rms error of about 2 m (4% of the length); this error decreases quite rapidly, and for N=25, the average rms error is only 1 mm.

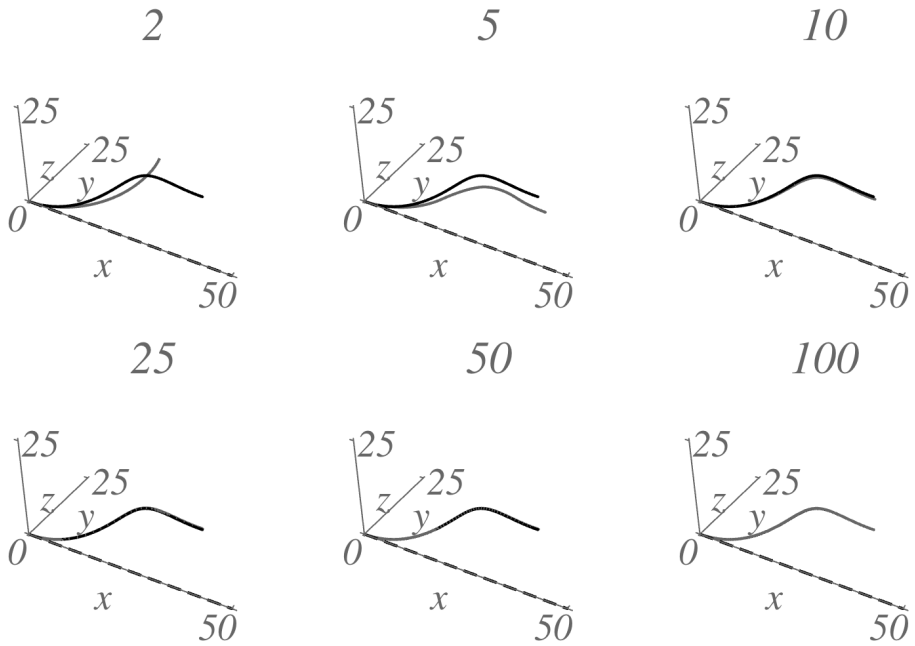

Fig. 3. Simulation #1 reconstruction results for various sensor counts.

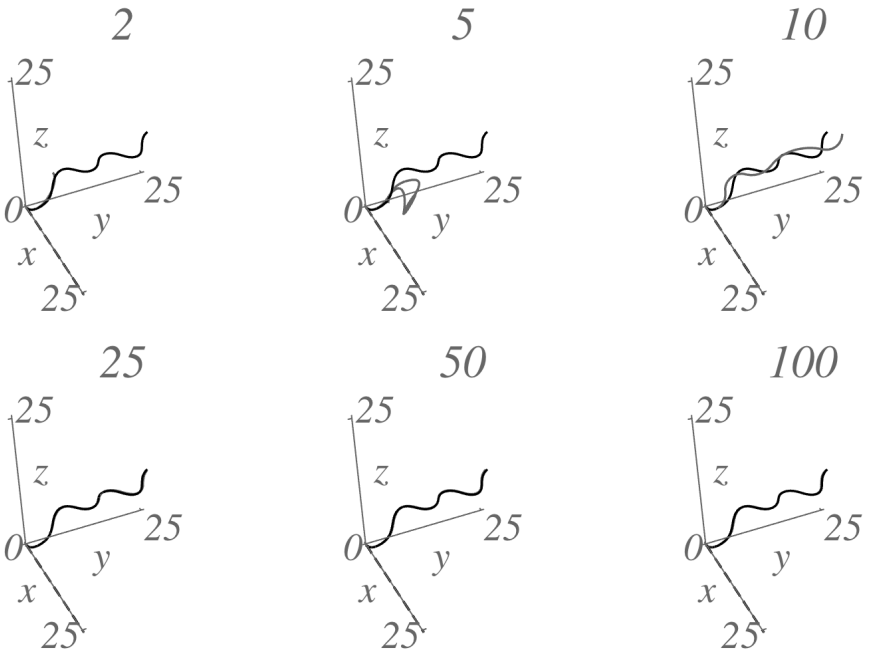

Fig. 4. Simulation #2 reconstruction results for various sensor counts.

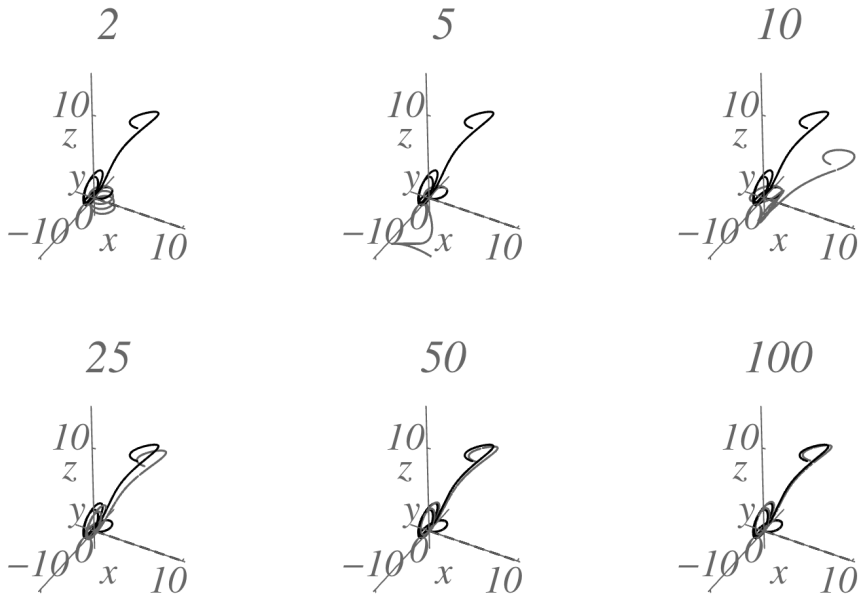

Fig. 5. Simulation #3 reconstruction results for various sensor counts.

Figures 4 and 5 show the same kind of results for two increasingly complex deformations with added stretch components and multiple curvature and torsion changes. The complexity increases naturally demand higher sensor counts before equivalent levels of accuracy are obtained, essentially 50 sensor locations for simulation #2 and 100 sensor locations for simulation #3. In all cases, however, the algorithm smoothly converges. The largest errors are typically at locations farthest from whatever location a boundary condition was imposed. In this work, it was assumed that the proximal end of the cylinder was at a known location (the origin); consequently, the error is maximal at the distal end. This propagation of error would be different if a known condition were imposed at a different location.

In practical applications, the measurements of strain from a real sensor array contain noise, and additionally other sources of external uncertainty can corrupt the algorithm's performance. To address robustness, Monte Carlo simulations on all three

shapes were performed with uniform noise added at both the [-5,5] microstrain and [-50,50] microstrain levels to each gage. The average root mean square error over the length of the cylinder between prediction and finite element simulation was computed for the first simulation only (for illustrative purposes) for a number of cross section sensor counts. Fig. 6 shows these results. The error is dominated by algorithm performance at very low sensor counts, but above about N=25, the error becomes more noise-dominated. For noise-free data, the algorithm approaches 0.001% of length in rms error for N=100.

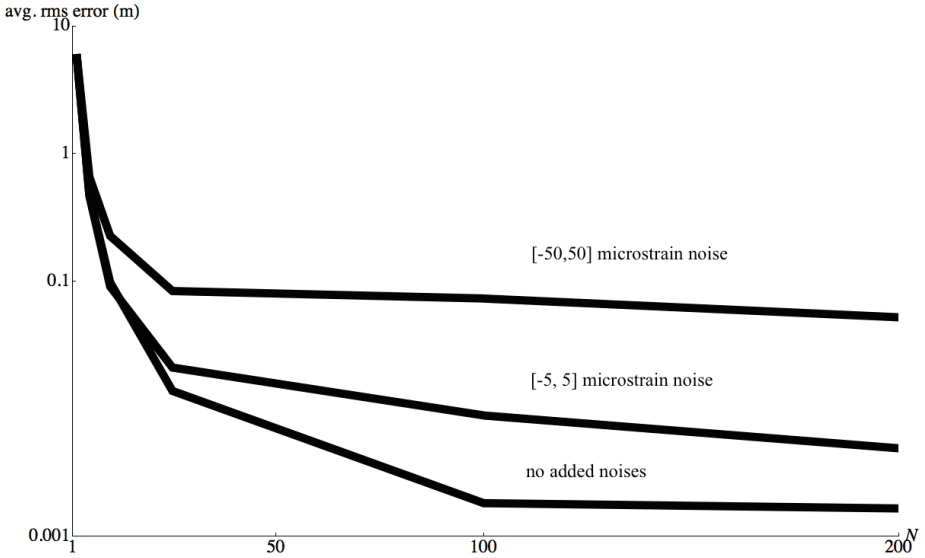

Fig. 6. RMS reconstruction error for different sensor counts for simulation case #1.

4. SUMMARY

This paper proposed a model-based method for obtaining the global three-dimensional displacement of rod-like structures from discrete strain measurements. The method utilizes a material-adapted reference and finds an analytical solution for local strain neighborhoods. The solution is robust to singularities and was validated with three finite element models of a 50 m hollow plastic cylinder undergoing significant three-dimensional deformations. Average rms errors of a few mm (hundredths of a percent of length) were obtained which were either noise- or sensor count-limited, depending on shape complexity. The approach has good applicability for embedded platforms, since the only computation involves a matrix inversion.

REFERENCES

[1] R. L. Bishop, "There is More Than One Way to Frame a Curve," *American Mathematics Monthly* 82(3), pp. 246-251, 1975.

[2] E. Cosserat and F. Cosserat, *Theorie des Corps Deformables*, Herman (Paris), 2001.

[3] A. E. H. Love, *A Treatise on Mathematical Theory of Elasticity*, Dover (New York), 1909.

[4] J. Langer and D. Singer, "Lagrangian Aspects of the Kirchoff Elastic Rod," *SIAM Review* 38(4), pp. 605-618, 1996.

[5] E. Reisner, "On Finite Deformations of Space-Cured Beams," *Journal of Applied Mathematics and Physics* 32, pp. 723-744, 1981.

[6] M. D. Todd, C. J. Stull, and M. Dickerson, "A Local Material Basis Solution Approach to Reconstructing the Three-Dimensional Displacement of Rod-Like Structures from Strain Measurements," *ASME Journal of Applied Mechanics*, 80(4), 041028(1-10), 2013.